Pressure Distribution in the Structure of a Propagating Current Sheet

THOMAS M. YORK
The Pennsylvania State University, University Park, Pennsylvania
AND
ROBERT G. JAHN
Princeton University, Princeton, New Jersey
(Received 2 July 1969; final manuscript received 15 December 1969)

The structure of the current sheet in a dynamic z pinch in argon is studied with a specialized high-speed piezoelectric pressure transducer capable of following profiles of axial and radial pressure within the discharge. Correlation of these data with electric and magnetic field profiles, luminosity, and voltage records, indicates three distinct zones within the sheet in sequence, regions of electron current conduction, mass accumulation with ion current conduction, and induced flow of unswept gas. Profiles of particle density, velocity, and temperature are evaluated on the basis of a simplified gas-kinetic model. The current sheet is found to entrain a large percentage of the gas encountered, and a momentum balance across the sheet is in approximate agreement with snowplow predictions, but the distributions of current and mass density differ categorically from conventional piston-shock wave models.

I. INTRODUCTION

Pulsed plasma accelerators are being studied as high performance space thrusters, fusion injectors, and solar wind simulators, as well as instruments for basic research on the properties of dense plasmas. In devices of this type an intense current sheet is accelerated by its self-magnetic field into an ambient body of gas contained in an appropriate discharge configuration, attaining velocities of the order of 10^4 m/sec. In a properly designed and operated accelerator, the propagating current sheet entrains a large fraction of the ambient gas, but the details of the entrainment process and the mass distribution within the sheet have so far evaded direct observation. Some aspects of the sheet structure have been inferred from interior electromagnetic field[1,2] and electron density[3] measurements, and elaborate theoretical calculations have been attempted.[4] This paper describes a series of experiments to probe the interior of a current sheet in argon with a high-speed, high-resolution pressure transducer, correlated with other diagnositics, to determine the profile of gas-kinetic pressure and thereby to infer the distributions of mass density and related properties.

II. APPARATUS AND CURRENT SHEET GEOMETRY

The propagating current sheet is generated in the closed-chamber linear pinch discharge device shown in Fig. 1, driven by a 50-μF pulse-forming network charged to 10 kV described in detail elsewhere.[5] The discharge chamber is 8 in. in diameter, has a 2-in. electrode spacing and is initially filled with

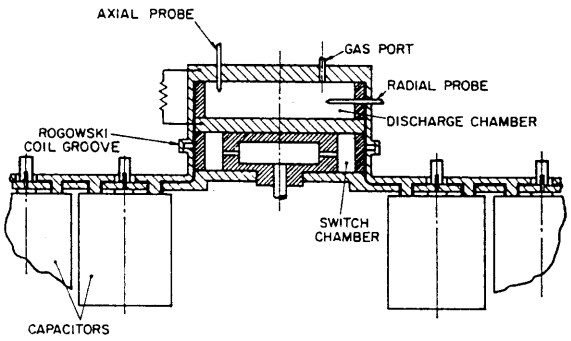

FIG. 1. Pinch discharge apparatus (schematic).

argon at a uniform pressure of 0.1 Torr. The circuit current waveform, shown in Fig. 2, is tailored empirically to provide a constant velocity, constant current density sheet over its radial incursion.

Also shown in Fig. 2 is a series of radial-view Kerr-cell photographs, taken through the sidewall Pyrex insulator, via an opening in the outer return conductor. Magnetic probe records taken simultaneously with such data indicate that the visible luminous fronts correspond closely to the positions of the current sheet. Departure from the ideal cylindrical sheet configuration is evident, both as a diffusion of its structure near the anode and to a lesser extent near the cathode, and as a slight inclination of the sheet with respect to the axis. However, the portion of the current sheet near the center plane is found to be well-defined and stable, and over the radial excursion from 3 to 1.5 in. maintains a current density of about 10^8 A/m^2, a thickness of about 1.5 cm, and a constant radial

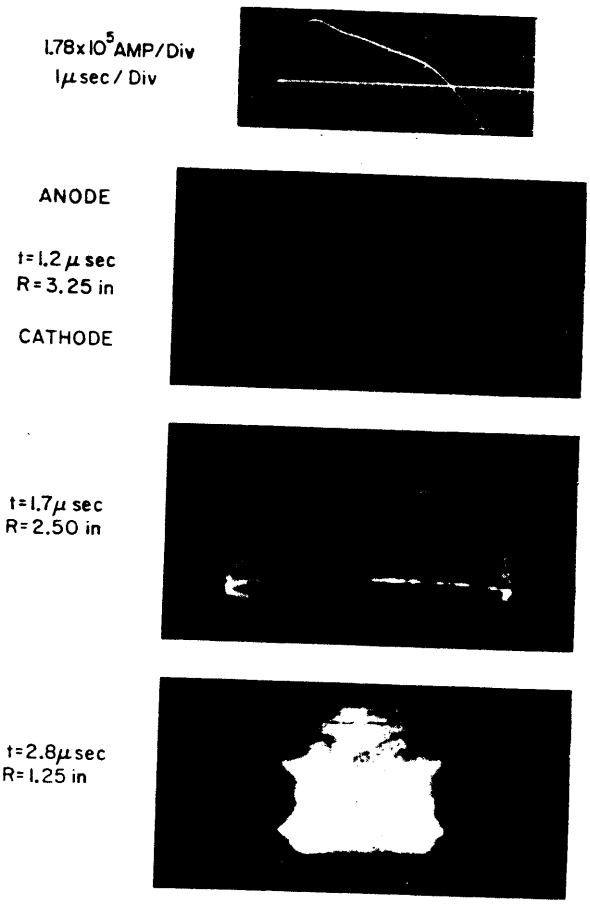

FIG. 2. Circuit current waveform and radial view photographs of pinch discharge.

velocity of about 3×10^4 m/sec. All of the subsequent experiments are confined to this mid-electrode portion of the sheet.

III. PRESSURE PROBE DEVELOPMENT

An ideal probe for the desired measurement would faithfully respond to the profile of gas-kinetic pressure in the passing current sheet with a linear output, free of spurious signal, while negligibly disturbing the local sheet structure. For the sheet intensity, width, and velocity involved here, this translates into requirements of millimeter spatial resolution, tenth-microsecond rise time, and a linear sensitivity of at least 0.1 mV/Torr, uncompromised by the electromagnetic noise from the adjacent discharge. The state-of-the-art performance of various existing pressure probes applicable to plasma studies, as recently surveyed by Jones and Vlases,[6] does not meet the above requirements. Several attempts have been made to probe transient discharges of this type with direct-contact piezoelectric devices,[7,8] but these served only to define nominal time-of-arrival of relatively large pressure pulses. To follow details of the pressure profiles on a submicrosecond time scale requires the development of a highly specialized probe with response characteristics superior to those previously developed.

Briefly,[9] the probe concept found to be optimum for this application involves a piezoelectric ceramic element separated from the plasma by a minimum thickness of insulation, and suitably supported by a structure of backing rod, coaxial electrode connections, and an insulated housing as shown in Fig. 3. The most critical aspect of probe design affecting the linearity of its response is the proper matching of the backing rod to that of the piezoceramic. The common practice of matching the acoustic impedance of the two elements to minimize the thickness mode stress oscillations was found to be inadequate. Specifically, using PZT 5-A ceramic elements (Clevite Corp., Cleveland, Ohio) with brass, tin, and nonpolarized PZT 5-A backing elements, the internal thickness oscillations changed little while the radial mode oscillations dominated the probe response. An analytical and experimental study of the stress conditions across the crystal-backing rod interface indicated that the lateral strain condition was the most critical factor, and that radial stress wave distortion could be reduced by keeping the quotient of Poisson's ratio by Young's modulus in the backing rod as large as possible compared to the same quotient in the ceramic element, i.e., the backing rod should serve to damp the radial oscillations. Stainless steel was found to be the best common material from this standpoint.

The prototype transducers use ceramic elements 0.010-in. thick, 0.15625-in. (4 mm) in diameter, encased in the insulated coaxial arrangem

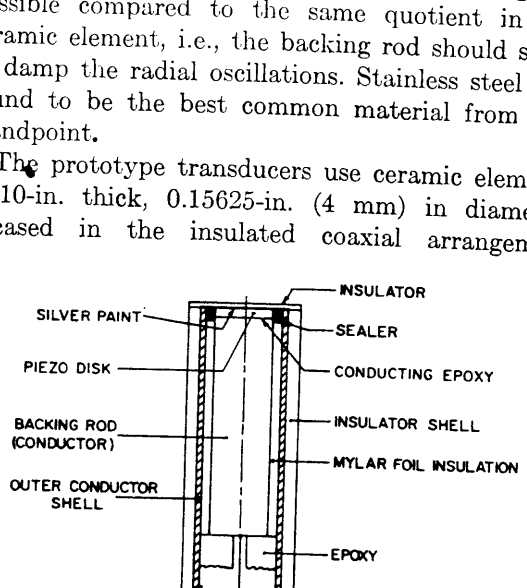

FIG. 3. Piezoelectric pressure transducer (schematic).

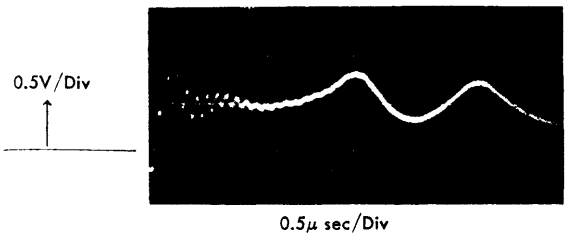

FIG. 4. Pressure probe response to reflected shock.

shown in Fig. 3. A 0.3125-in. o.d. Pyrex encased unit is used for radial probing and a 0.5-in. o.d. nylon encased unit for axial probing. The electrical insulation on the crystal face consists of one layer of 1-mil thick Scotch No. 74 insulating tape covered with one thin layer of Zapon Aquanite (Glidden) lacquer. The response of this type probe to head-on reflection of a shock wave in a shock tube is shown in Fig. 4. The high-frequency oscillations are due to thickness mode stress propagation and can be ignored in evaluation of the real-pressure mean response. The onset of the more objectionable lower-frequency radial mode oscillation is delayed until about 1.5 μsec, allowing reasonable measurements of pressure to be made within that interval. Calibration was carried out over a range of reflected shock waves in 0.5 Torr to 1.0 atm argon, producing pressure differences up to 5.2 atm; over the entire range the probe response was linear with pressure increase. To preserve the frequency response, the probing unit is coupled with a battery-powered cathode follower when used within the discharge.

IV. PRESSURE PROBE—CURRENT SHEET INTERACTION

In order to examine the current sheet away from the electrode surfaces, for the reasons discussed in Sec. II, the body of the probe projects into the chamber. Interpretation of its response thus must be based on some understanding of the interaction of the current sheet with the probing body. Figure 5 displays Kerr-cell photographs of the luminosity patterns developed over the radial probing shape at $R = 2$ in. midplane. After the passage of the well-defined rear surface of sheet luminosity, a form of detached "bow wave" appears shrouding the bluff probe end, perhaps indicative of a residual gas flow behind the sheet. Similar luminous waves are observed on the upstream (stagnation) side of the axial probe body. In the hope of reducing spurious diffraction signals on the sensing surface of the axial probe, it was first fitted with a sharp-leading-edge annular collar. Photographs of the

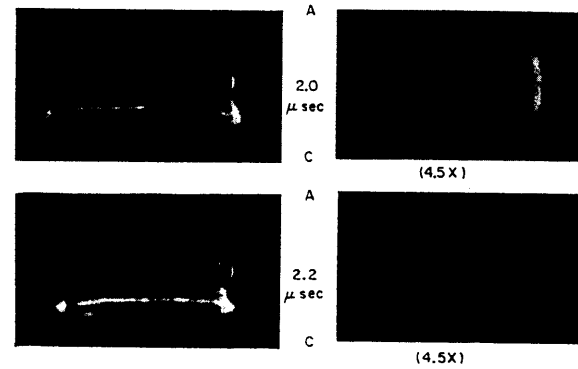

FIG. 5. Luminosity patterns about radial probe. (Magnified details presented on the right side.)

sheet-induced flow over this configuration are shown in Fig. 6. Note that a luminous wave is still visible over the sensitive probe surface, and further, that the wave–surface angle is distinctly different for the probe mounted on the cathode than for that mounted on the anode. Such behavior suggests that flow deflection occurs at the leading edge in each case, and is perhaps indicative of a flow inclination associated with the slightly tilted sheet.

A complementary factor to be considered is the effect of the probe body, and any appendages to it, on the distribution of current density within the sheet. Figure 7 shows simultaneous records of axial pressure and magnetic induction change, $\dot{B}_\theta$, —here essentially proportional to local current density—taken with several different probing shapes. Note that the distortion in current density profile caused by a "flow isolator" far outweights any improvement in the pressure response, indicating that a bare probe, without isolator, is the optimum arrangement for obtaining undistorted, well-correlated measurements.

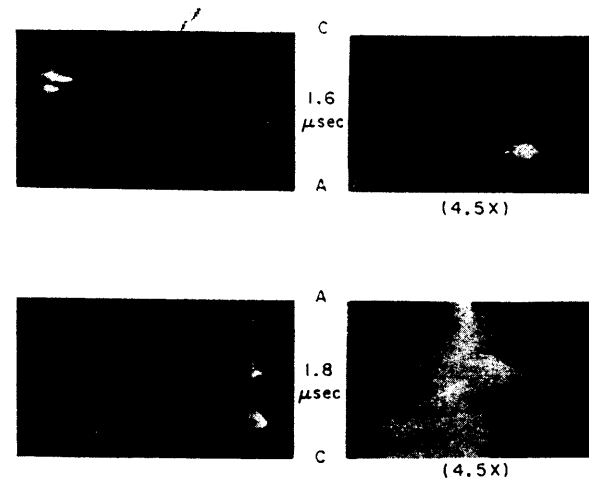

FIG. 6. Luminosity patterns about axial probe with flow isolator. (Magnified details presented on the right side.)

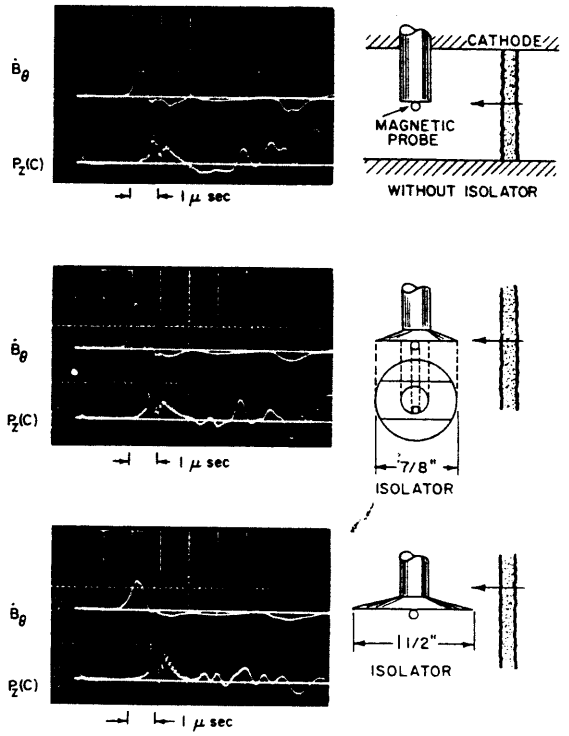

FIG. 7. Effect of flow isolator on probe response (R = 2 in.; h = 1 in.).

V. EXPERIMENTAL DETERMINATION OF CURRENT SHEET PROFILES

The current sheet structure is probed with the pressure-sensing instruments described above, with magnetic induction coils, and with double electric field probes. Circuit current is measured with an external Rogowski loop. The magnetic probes of Formvar-coated copper wire with 2.4-mm coil diameter, are mounted on the pressure probe body, directly adjacent to the pressure-sensing surface to insure exact time correlation. The electric field probes are conically shaped with a 2.5-mm diam ring electrode separated by a 1.85-mm gap from a tip electrode of equal area. Data are recorded with the axial pressure probe inserted through the anode and the cathode (Fig. 6). The axial and radial probes are separated by a 30° azimuthal angle to avoid mutual distortion; tests made with the probes arranged in several different relative positions confirmed that such a configuration allowed precise time correlation of the data. Three separate discharges are required to acquire complete data at any one point in the chamber; the magnetic probe measurement is repeated as a control. Typical results, time-correlated using the common $\dot{B}_\theta$ signal, are presented in Fig. 8.

On the basis of such data, we identify three regions of interaction in the current sheet structure:

Region I is characterized by intense current conduction, isotropic pressure response of relatively small magnitude, and measurable axial and radial electric fields.

Region II is characterized by relatively small current density, a strong, discontinuous radial pressure response, and different magnitudes of axial pressure depending on the probe orientation.

Region III is characterized by negligible current density and radial pressure response, approximately equal axial pressures, and strong axial electric field and azimuthal magnetic fields.

Two features of this structural pattern are of particular significance: (1) There is a distinct delay (~0.2

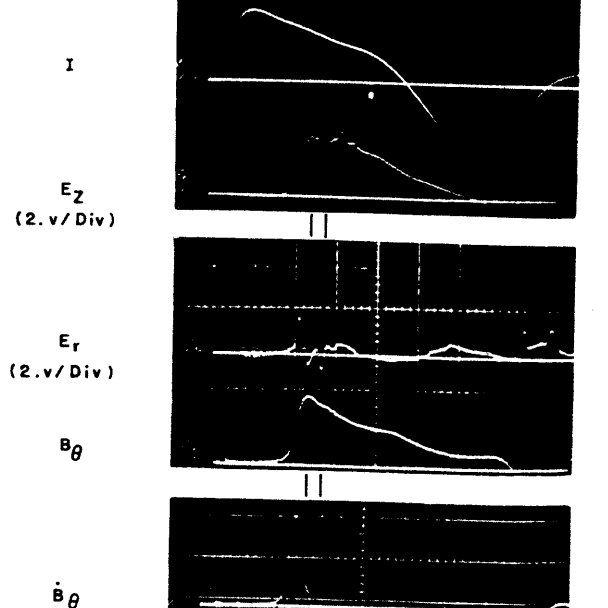

FIG. 8. Responses of electric, magnetic, and pressure probes to passing current sheet.

μsec) between the $\dot{B}_\theta$ peak and the sharp pressure rise, implying a corresponding spatial separation of 0.6 cm between the position of maximum current density, and the leading edge of the accumulated mass. (2) The abrupt pressure rise is quickly followed by a rapid expansion, implying that the accumulated mass is confined to a narrow layer, ~0.1 cm thick.

Similar data obtained at other radii between 3 and 1.5 in. indicate that all measured properties in each of the three regions remain virtually constant as the sheet implodes, with the exceptions of the radial pressure in region II which increases with sheet progression, and the separation between $\dot{B}_\theta$ peak and pressure discontinuity, which also increases.

VI. EVALUATION OF FIELD AND PARTICLE KINETIC PROFILES IN THE SHEET

Reduction of magnetic and electric probe records to profiles of current density and electric field proceeds in standard fashion, but extraction of gas-kinetic pressure profiles from the piezoelectric signatures involves consideration of both electrostatic sheath and gasdynamic effects.[9] The degree of ionization within the current sheet can be estimated from measurements of voltage drop across the sheet discharge. Presuming electron current carriers, the corresponding energy increment is balanced with energy loss by inelastic collision to indicate a mean electron temperature of about 4 eV, a value compatible with an assumption of full single ionization near the sheet leading edge. Further, indicated values of radial electric field are consistent with charge balance, so $n_i \approx n_e$. On this basis, full single ionization, with $n_i = n_e$ will be assumed throughout the analysis.

Regarding the sheath effect, a momentum analysis of particles streaming between the plasma and the probe surface indicates that the pressures sensed by the piezoelement are equal to the gas-kinetic pressure in the plasma. An exact analysis of the gasdynamic interaction is not possible because of the transient nonequilibrium nature of the event, but these effects can be estimated to establish approximate relationships. The transient character of the interaction, along with estimates of local plasma properties, indicate that effective "cold wall" conditions prevail, i.e., the characteristic time for thermal transport is of the order of that for fluid dynamic adjustments, suggesting that Newtonian analysis may be applicable. At worst, such an approach should serve to correlate first-order effects.

In this spirit, the determination of static pressure within the various zones of the sheet can be carried out as follows. In region I, the radial pressure probe response P_R and the responses of the axial probe inserted through the cathode $P_z(C)$ and anode $P_z(A)$ are essentially the same, implying that each responds primarily to the local static pressure with negligible gasdynamic disturbance, e.g.,

$$P_s \approx P_z \qquad \text{(region I)}.$$

For region II, where $P_R \gg P_z(C) \gg P_z(A)$, the static pressure can be evaluated from comparison of the radial and axial probe responses via

$$P_R \approx n_i m_i V_s^2,$$

$$P_z(C) \approx P_s + n_i m_i (V_s \sin \phi)^2 \qquad \text{(region II)},$$

where V_s is the sheet speed, ϕ its angle of tilt, n_i and m_i are the ion number density and mass, and $P_z(C)$ is corrected for the effects of zone II thickness relative to the piezoelement size. In region III $P_z(C) \approx P_z(A)$, again permitting the identification

$$P_s \approx P_z \qquad \text{(region III)}.$$

The sheet pressure profiles computed from these relations are presented in Fig. 9.

The pressure data can be incorporated into the sheet structure analysis in the following manner:

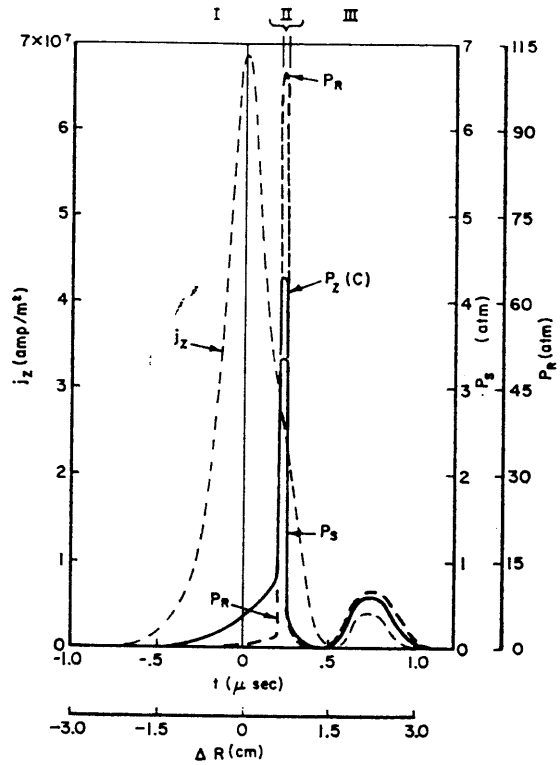

FIG. 9. Current density, radial and axial pressure profiles (R = 2 in., h = 1 in., t = 2 μsec).

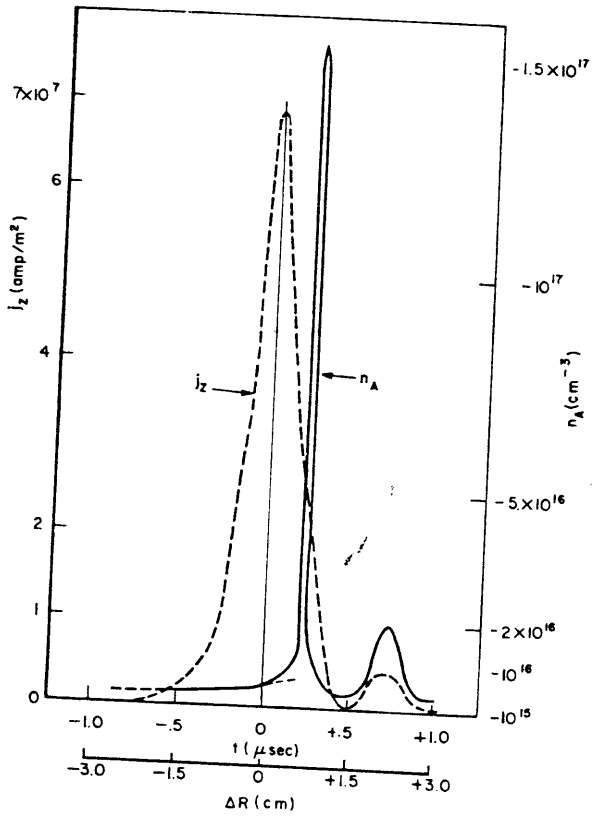

FIG. 10. Number density and current density profiles ($n_0 = 3 \times 10^{15}$ cm^{-3}, $R = 2$ in., $h = 1$ in., $t \approx 2$ μsec).

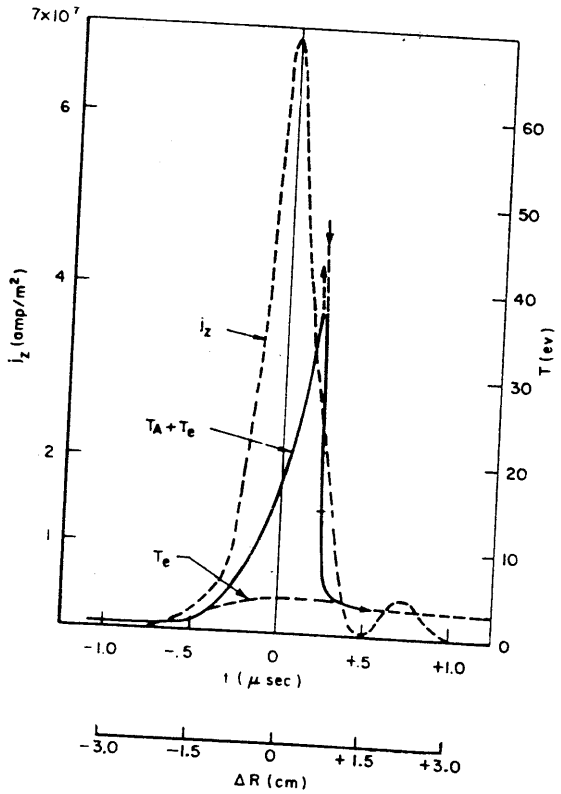

FIG. 11. Temperature and current density profiles ($R = 2$ in., $h = 1$ in., $t \approx 2$ μsec).

The radial pressure is related to ion number density and streaming velocity, v_R by $P_R = n_i m_i v_R^2$ and the axial (static) pressure is related to the gas-kinetic temperatures through an equation of state involving ion and electron temperatures, e.g.,

$$P_s = nk(T_i + T_e).$$

Ion velocities in region I may be estimated from collisionless energetics through the radial electric field; the radial velocity of the particles in the entrained zone (II) is defined as the measured sheet speed $v_R = V_s$; in region III with negligible current density and an estimated moderate conductivity $v_R \approx E_Z/B_\theta$. The density profile estimated by the above procedures is presented in Fig. 10; the temperature profile indicated by combining the pressure and density in the equation of state is presented in Fig. 11. The ion density profile is related to a sweeping parameter S defined as the ratio of entrained mass to that originally in the volume swept by the sheet, which can be expressed in the form

$$S = \left(\frac{n_{II}}{n_0} - 1\right) \frac{2R\,\delta}{(R_0^2 - R^2)},$$

where δ is the thickness of region II with density n_{II}, n_0 is ambient density, and R_0 is chamber radius; δ is determined from the reduction of axial pressure response time during the sheet sweeping event. Typically, $V_s = 3 \times 10^4$ m/sec, $\delta = 1.2$ mm, $n_{II} = 1.6 \times 10^{17}$ cm^{-3}, and $S = 0.90$ indicating an efficiently sweeping sheet.

VII. DISCUSSION OF CURRENT SHEET STRUCTURE AND DYNAMICS

The intense current conduction in region I can be described by a generalized Ohm's law,

$$\mathbf{j} = \sigma_0\left(\mathbf{E} + \mathbf{v}\times\mathbf{B} + \frac{\nabla p_e}{n_e e} - \frac{\mathbf{j}\times\mathbf{B}}{n_e e}\right).$$

From experimental data, the electron pressure gradient is negligible, and further $j_R \approx \phi j_Z \ll j_Z$, so that

$$j_{Ze} \approx \frac{n_e e E_R}{B_\theta}.$$

Estimating radial ion velocity to indicate number density as outlined above, and using measured values of E_R, B_θ it is found that the bulk of the current in region I is carried by electrons:

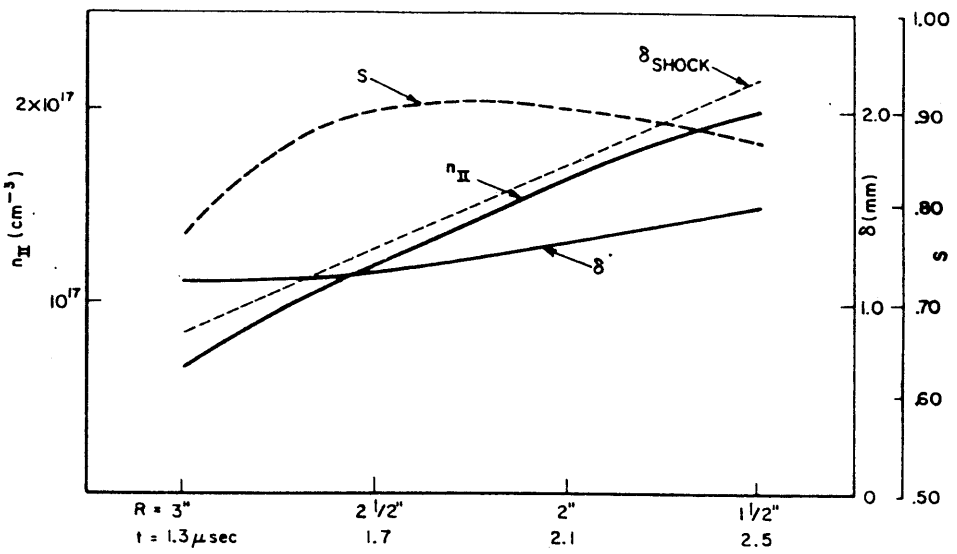

FIG. 12. Radial variation of peak density, width of entrained zone, and sweeping efficiency.

$$j_z(I) \approx j_{ze}.$$

The radial electric field in region I appears to be the mechanism for transfer of $\mathbf{j}\times\mathbf{B}$ force density from the electrons to the ions.

A radial momentum balance across the current sheet profile results in the relationship,

$$P_{iB} \equiv \int_{R_1}^{R_2} j_z B_\theta \, dR \approx \rho_0 V_s^2 S.$$

Taking typical values, the particle kinetic pressure of the entrained gas P_S is comparable to the electromagnetic pressure supporting the sheet system P_{iB}. In fact, typical values of the latter imply $S > 1$, an indication that a correct momentum balance must include wall (electrode) momentum losses.

The radial variation of n_{II}, δ, and S provides another indication of the nature of the acceleration process and is presented in Fig. 12. It can be seen that the density of the entrained gas increases with sheet incursion, while the thickness δ remains constant. Other details of the current sheet structure have already been shown to be incompatible with the motion of a separated piston-shock system, but for purposes of comparison the predicted separation of piston and shock δ_{shock} in such a model with $V_{piston} \equiv V_s$ is also presented in Fig. 12.

VIII. SUMMARY

The compatible evaluation of pressure, magnetic field, and electric field measurements has indicated that argon gas acceleration by a propagating current sheet occurs in three distinct phases: a leading region of intense electron current conduction, producing full gas ionization with subsequent radial and axial ion acceleration in radial electric fields and azimuthal magnetic fields; a following narrow region of intense mass concentration, with axial ion streaming that correlates well with the observed low level current conduction; and a "wake" region of induced ionized-gas flow, following the intense discharge with fractional sheet velocity. Analysis of the data provides profiles of pressure, density and temperature through the three regions, and indicates a high degree of mass entrainment by the sweeping current sheet.

ACKNOWLEDGMENTS

The authors wish to thank W. von Jaskowsky, A. L. Casini, and J. D. Tregurtha for their help in performing the experiments and interpreting the results.

This work was performed at Princeton University under the support of the National Aeronautics and Space Administration Grant NGL-31-001-005.

[1] L. C. Burkhardt and R. H. Lovberg, Phys. Fluids **5**, 341 (1962).
[2] R. L. Burton and R. G. Jahn, Phys. Fluids **11**, 1231 (1968).
[3] W. R. Ellis, Jr., Ph.D. thesis, Princeton University (1967).
[4] K. Hain, G. Hain, K. V. Roberts, S. J. Roberts, and W. Köppendörfer, Z. Naturforsch. **15a**, 1039 (1960).
[5] N. A. Black, Ph.D. thesis, Princton University (1966).
[6] T. G. Jones and G. C. Vlases, Rev. Sci. Instr. **38**, 1038 (1967).
[7] N. V. Fillipov, in *Plasma Physics and the Problems of Controlled Thermonuclear Reactions* (Pergamon Press, Inc., New York, 1959), Vol. 3, p. 280.
[8] G. C. Vlases, Phys. Fluids **10**, 2351 (1967).
[9] T. M. York, Ph.D. thesis, Princeton University (1968).